PAPER

Exceptionally high temperature spin crossover in amide-functionalised 2,6-bis(pyrazol-1-yl)pyridine iron(II) complex revealed by variable temperature Raman spectroscopy and single crystal X-ray diffraction†

Max Attwood, [ID] [a] Hiroki Akutsu, [ID] [b] Lee Martin, [ID] [c] Toby J. Blundell, [ID] [c] Pierre Le Maguere[d] and Scott S. Turner [ID] *[a]

The synthesis of a novel amide-functionalised 2,6-bis(pyrazol-1-yl)pyridine-4-carboxamide ligand (**bppCONH₂**) is described. The complex salts [Fe(**bppCONH₂**)₂](BF₄)₂ and [Fe(**bppCONH₂**)₂](ClO₄)₂ were synthesised and characterised by SQUID magnetometry, differential scanning calorimetry, variable temperature Raman spectroscopy and single crystal X-ray diffraction. DSC measurements of [Fe(**bppCONH₂**)₂] (BF₄)₂ indicate a spin-crossover (SCO) transition with $T\uparrow$ at 481 K and $T\downarrow$ at 461 K, showing a 20 K hysteresis. DSC for the perchlorate salt shows an SCO transition with $T\uparrow$ at 459 K and $T\downarrow$ at 445 K with a 14 K hysteresis. For the BF_4^- salt analysis of low and high-spin state crystal structures at 101, 290 and 500 K, suggest stabilisation of the low spin state due to the formation of 1D hydrogen-bonded cationic chains. Variable temperature Raman studies of the BF₄ salt support the presence of a high temperature SCO. It is speculated that the presence of hysteresis may be attributed to differences in the inter-molecular hydrogen bonding in the low spin and high spin states.
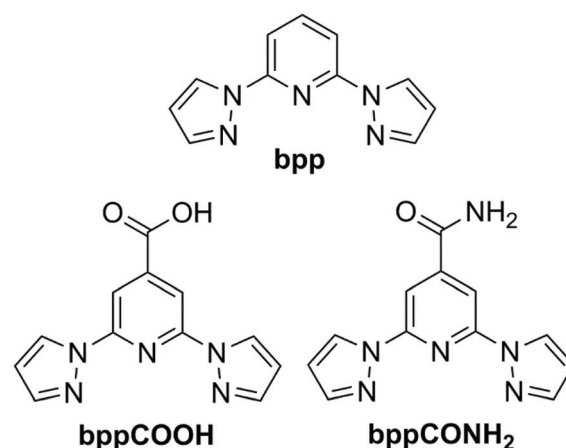
Introduction

A series of ligands based on 2,6-bis(pyrazolyl)pyridine (**bpp**, Scheme 1) have proven reliable for producing Fe(II) complexes with spin-crossover (SCO) and thermal hysteresis.[1–3] Typically the transition temperatures are in the range *ca.* 200–270 K, although these temperatures have been successfully enhanced by substitution at the pyridyl's 4 position through moderating intermolecular interactions. For example, structural analysis of [Fe(**bppCOOH**)₂](ClO₄)₂ indicated that hydrogen bonding between Fe complex cations is likely responsible for increasing the SCO transition temperature to 380 K, while maintaining

cooperativity.[4] In other words, by stabilising the low spin state relative to the high spin state. Functionalising with carboxylate groups produces cationic 1D chains, facilitating an abrupt SCO transition without relying on intermolecular π–π-stacking interactions. The latter interactions are prominent in other **bpp**-based salts which have the so-called 'terpyridine embrace'

[a]Department of Chemistry, University of Surrey, Guildford, GU2 7XH, UK.
E-mail: s.s.turner@surrey.ac.uk
[b]Department of Chemistry, Graduate School of Science, Osaka University,
1-1 Machikaneyama, Toyonaka, Osaka 560-0043, Japan
[c]School of Science and Technology, Nottingham Trent University, Clifton Lane,
NG11 8NS, UK
[d]Rigaku Americas Corporation, 9009 New Trails Drive, The Woodlands, TX 77381,
USA

†Electronic supplementary information (ESI) available: Further experimental details of ligand synthesis, TGA of complexes (Fig. S1), variable temperature powder XRD of [Fe(**bppCONH₂**)₂](BF₄)₂ (Fig. S2). CCDC 2085819–2085821 and 2085826. For ESI and crystallographic data in CIF or other electronic format see DOI: 10.1039/d1dt01743h

Scheme 1 Ligands discussed in this report and associated abbreviations.

structural motif.[5] It is proposed that forming 1D cationic chains is a robust method of producing compounds with SCO above room temperature. Furthermore, modifying the hydrogen-bonded network may provide a means to fine-tune the SCO transition temperature and cooperative nature.

The highest reported low-spin (LS) to high-spin (HS) transition temperature for a monomeric Fe(II) complex with ligands derived from **bpp** is $T_{1/2}$ = 440 K,[6,7] where $T_{1/2}$ is the temperature at which there is a 1 : 1 ratio of LS and HS states. However, this transition is not reversible. The compound is a polymorph of [Fe(**bppCCH**)$_2$](BF$_4$)$_2$, which achieves this transition temperature on a heating cycle from 330 K. However, on subsequent cooling there is an irreversible transition to a different polymorph that has an SCO centred at 340 K. By contrast the highest temperature for a reversible SCO that we were able to find was at 406 K for [Fe(**bpp-pyridine-3-yl**)$_2$](ClO$_4$)$_2$, with the BF$_4^-$ salt not far below at 400 K.[8] In both cases no thermal hysteresis is observed.

To further investigate the effect on SCO of moderating interactions between cationic chains we previously synthesised the **bpp** 4-substituted thioamide derived ligands **bppCSNH$_2$** and **bppCSNHMe**.[9] The Fe(II) complexes of **bppCSNHMe** have 1D chain structures and show SCO at relatively high temperatures: 332 K (BF$_4^-$ salt) and 325 K (ClO$_4^-$ salt). The route to these ligands requires synthesis of the corresponding amides, and this report describes the synthesis of the ligand **bppCONH$_2$** (Scheme 1) and the SCO behaviour of its Fe(II) salts.

It is thought that the bi-functional nature of the NR$_2$ group could also facilitate future derivatisation, without significantly affecting the metal core. To our knowledge, only one amide derivative has been previously reported and investigated in terms of the magnetic properties,[10,11] while another pyrazolyl-functionalised derivative has been investigated for its luminescent properties.[12] In the former work, the compound [Fe(**bppC(O)NHC(CH$_2$OH)$_3$**)$_2$](BF$_4$)$_2$ underwent a very gradual SCO transition with $T_{1/2}$ slightly above 400 K. Although cationic chains were formed, there was a lack of intra-chain OH⋯OH hydrogen bonding, and only O⋯NH hydrogen bonds connected adjacent members of each chain. Notably, Raman spectroscopy provided supporting evidence for the SCO transition, a technique that has been widely used to monitor SCO, including with other **bpp** variants. For example, the Chandrasekar group used this technique to characterise the thermally induced SCO in nano-tapes of a coordination polymer with a **bpp**-like coordination environment. In this case they worked with a 488 nm laser[13] by identifying a band at 1017 cm^{-1} corresponding to the LS state. This is consistent with a report by the Ruben group which used a 633 nm excitation source at 170 and 393 K to characterise the SCO of complexes of pyridine-functionalised **bpp** derivatives following lithographic printing onto a silicon surface.[14] Shepherd et al. studied Raman spectra of monomeric and dimeric Fe complexes containing **bpp** derivatives under both variable temperature and pressure.[15,16] Due to limitations of our instrumentation, which is only able to measure magnetic data up to 400 K, we have used Raman spec-

troscopy, single crystal X-ray diffraction and DSC to characterise the high temperature SCO described in this work.

Experimental

Physical measurements

CHN elemental analysis was performed using an Exeter Analytical Inc. CE-440 Elemental Analyser. Differential scanning calorimetry (DSC) and thermal gravimetric analysis (TGA) were performed using TA Instruments DSC Q1000 and TGA Q500, respectively. Samples for DSC were placed inside a hermetically sealed aluminium pan and heated at a rate of 10 K min^{-1}. Analysis of this data was performed in TA Universal software. NMR was performed using a Bruker AVII400NMR instrument. Magnetic properties were measured using a Quantum Design MPMS2 magnetometer on powders in aluminium foil sample holders or quartz tubes. Corrections were made for the sample holders and the compound's diamagnetic contribution was estimated using Pascal's constants.[17] Single crystal X-ray diffraction for BF$_4$ salts were predominantly measured using a Rigaku Rapid II imaging plate system with MicroMax-007 HF/VariMax rotating-anode X-ray generator and confocal monochromated Mo-Kα radiation. The crystal structure at 500 K was measured with a Rigaku XtalLAB SynergyS system with a HyPix-6000HE detector and Cu-Kα radiation. No sample degradation was observed by re-measuring and checking the unit cell on cooling back to room temperature after collection at 500 K. The structure of the perchlorate salt was measured using a Rigaku Oxford Diffraction Excalibur System equipped with a Sapphire detector. High resolution mass spectrometry (HRMS) was performed using an Agilent 1260 Infinity II coupled to an Agilent 6550 Quadrupole time-of-flight mass spectrometer using electrospray ionisation in positive mode. Variable temperature Raman spectroscopy was performed using a Renishaw InVia Raman microscope with a 633 nm laser, CCD detector, holographic notch filters and diffraction grating. Samples were mounted on an enclosed Peltier heating stage within a nitrogen atmosphere. The Raman laser power was attenuated to 1% even though at 10% there was no visible damage to the sample surface. During the Raman data collection, the measurement had to be occasionally paused to re-centre the sample and/or re-focus the microscope.

Synthesis

All reagents, unless otherwise stated, were used as supplied without further purification. Scheme 2 shows the synthetic pathway used to generate the ligand **bppCONH$_2$**. 2,6-Dichloropyridine-4-carboxylic acid was synthesised according to Adamczyk et al.,[18] which was subsequently used to synthesise **bppCOOH** according to Vermonden et al.[19]

Synthesis of 2,6-bis(pyrazol-1-yl)pyridine-4-carboxamide (bppCONH$_2$)

A solution of SOCl$_2$ (10 ml) and **bppCOOH** (0.8171 g, 3.2 mmol) was reacted at 75 °C for 4 h under reflux, capped

Dalton Transactions

Paper
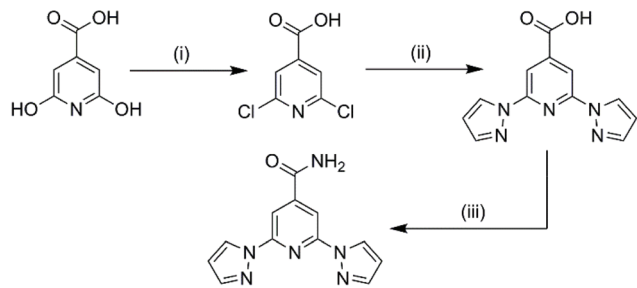
Scheme 2 Overview of synthetic procedures. (i) $POCl_3$, 140 °C, 24 h; (ii) NaH, pyrazole, 130 °C, 5 days; (iii) $SOCl_2$, 75 °C, 4 h, conc. NH_4OH.

with a $CaCl_2$ guard. Excess $SOCl_2$ was removed *in vacuo* and the resulting brown solid was dissolved in THF (25 ml). This solution was slowly added to conc. NH_4OH (10 ml) while stirring. The mixture was sealed and left for 2 h. The solvent was removed *in vacuo* giving a light brown solid. Recrystallization at −20 °C from a saturated solution in methanol gave a white microcrystalline solid. Yield: 0.716 g, (88%). ^{1}H NMR (400 MHz, DMSO): δ 8.99 (d, J = 2.6 Hz, 2H), 8.57 (s, 1H), 8.22 (s, 2H), 7.92 (d, J = 7.3 Hz, 2H), 7.88 (s, 1H), 6.67 (dd, J = 2.4 Hz, J = 1.8 Hz, 2H). ^{13}C NMR (400 MHz, DMSO): δ 165.62, 150.64, 148.41, 143.42, 128.84, 109.19, 107.55. HRMS (positive scan) m/z calculated = 255.0989 (M + H)$^+$, 277.0808 (M + Na)$^+$; Found = 255.0992 (M + H)$^+$, 277.081 (M + Na)$^+$, Na from eluent.

Synthesis of $[Fe(bppCONH_2)_2](ClO_4)_2$

Caution! Although we have experienced no practical difficulties during synthesis, metal perchlorates in the solid state, subject to heat, are potentially explosive. All such reagents and products are best kept in a cool place and out of direct sunlight.

$Fe(ClO_4)_2 \cdot 6H_2O$ (0.067 g, 0.185 mmol) was added to a solution of **bppCONH$_2$** (0.094 g, 0.37 mmol) in MeCN (10 ml). The solution was refluxed under N_2 for 20 minutes and concentrated by rotary evaporation to *ca.* 5 ml. The solution was filtered and decanted into a 20 ml scintillation vial. Vapour diffusion of Et_2O over 4 days yielded light orange/brown needle-shaped crystals. Yield: (0.11 g, 68%). Calculated for $C_{26}H_{24}Cl_2FeN_{12}O_{10}$: C, 39.47; H, 3.06; N, 21.24. Found: C, 39.16; H, 2.92; N, 21.2.

Synthesis of $[Fe(bppCONH_2)_2](BF_4)_2$

The same procedure as with $[Fe(bppCONH_2)_2](ClO_4)_2$ was used, substituting $Fe(BF_4)_2 \cdot 6H_2O$ (0.1027 g, 0.304 mmol) and **bppCONH$_2$** (0.1547 g, 0.609 mmol) in MeCN (10 ml). Vapour diffusion with Et_2O afforded red needle-shaped crystals. Yield: 0.129 g, (57%). Calculated for $C_{24}H_{20}N_{12}O_2B_2F_8Fe$: C, 39.06; H, 2.72; N, 22.78. Found: C, 39.57; H, 2.85; N, 23.42.

Results and discussion

Synthesis

Synthesis of **bppCONH$_2$** was afforded in reasonable yield and the ligand was recrystallised from methanol since it was rela-

tively insoluble in most other organic solvents. The ^{1}H-NMR spectrum of **bppCONH$_2$** shows two distinct N–H singlet peaks with chemical shifts differentiated by the relative proximities to the neighbouring oxygen atom. Reaction of the ligand with $Fe(BF_4)_2$ or $Fe(ClO_4)_2$ in a 2 : 1 ratio, followed by slow diffusion of Et_2O yields orange/brown or red crystals, typical colours of Fe(II) complex salts of **bpp**-type ligands in the LS state. Both $[Fe(bppCONH_2)_2]^{2+}$ salts are remarkably stable up to 250 °C according to TGA (Fig. S1†), above this temperature the BF_4^- salt begins to decompose. In contrast the ClO_4^- salt undergoes rapid oxidation, even under nitrogen, resulting in the formation of a black soot.

Description of the LS crystal structures

Single crystal diffraction measurements for $[Fe(bppCONH_2)_2](BF_4)_2$ were taken at 101 K, 290 K and 500 K, while $[Fe(bppCONH_2)_2](ClO_4)_2$ was analysed only at 293 K (LS state) due to its instability at elevated temperatures over a prolonged period *i.e.* during data collection. Both salts are isostructural at *ca.* 290 K, crystallising in the monoclinic $P2_1/n$ space group (Table 1). The asymmetric unit of the BF_4^- salt, at 101 K, is shown in Fig. 1. The cell volume of $[Fe(bppCONH_2)_2](ClO_4)_2$ is 2.2% larger than that of $[Fe(bppCONH_2)_2](BF_4)_2$ due to small increases in a- and b-cell lengths, attributed to the presence of the larger anions. Structures of the BF_4^- salt, at 101 K and 290 K exhibit average Fe–N$_{pyridyl}$ and Fe–N$_{pyrazolyl}$ bond lengths of 1.892–1.898 Å and 1.961–1.965 Å, respectively. These values are, consistent with the complex being in the LS state (Table 2). Similarly, at 293 K the perchlorate salt has Fe–N bond lengths that are consistent with the LS state (Table 2).

All structures at all measured temperatures reveals that the cations form 1D chains through amide hydrogen bonding. This is exemplified by $[Fe(bppCONH_2)_2](BF_4)_2$ at 101 K (Fig. 2) where the O1···N7 and O2···N1 distances measure 3.069 Å and 2.873 Å, respectively. The O2···N1 hydrogen bonds increase by 2.3% between 101 K and 500 K, while the O1···N7 interactions changes by just 0.7%, suggesting a lack of rigidity and asymmetry in the 1D chains. A further hydrogen bond is present in both salts between the amide group and anions constituting an anchoring-type interaction, such that BF_4^- or ClO_4^- anions occupy equivalent spaces in their respective structures.

Looking at a single hydrogen bonded 1D chain in either $[Fe(bppCONH_2)_2]^{2+}$ salt reveals wave-like motifs to the overall structure (Fig. 3, bottom). In comparison the structures of $[Fe(bppCOOH)_2]^{2+}$, first reported by Abhervé *et al.* for $[Fe(bppCOOH)_2](ClO_4)_2$,[4] and more recently by García-López *et al.* for $[Fe(bppCOOH)_2](BF_4)_2$,[20] show more linear 1D chains (Fig. 3, top), irrespective of the viewing direction. The wave-like motifs result from the more asymmetric hydrogen-bonded network compared to that in the **bppCOOH** salts.
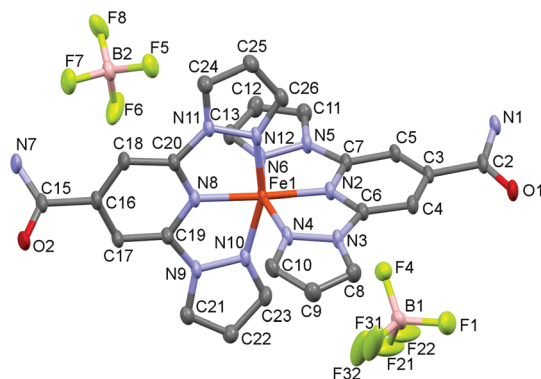
Crystal structure of HS $[Fe(bppCONH_2)_2](BF_4)_2$

The structure of $[Fe(bppCONH_2)_2](BF_4)_2$ was solved at 500 K, where it crystallises in the $P2_1/n$ space group. At 500 K, the structure is consistent with HS state Fe(II) compounds with average Fe–N bond lengths of 2.085 Å, approximately 8%

Table 1   Crystallographic data for Fe(II) coordination compounds of **bppCONH₂**

Compound	[Fe(**bppCONH₂**)₂](BF₄)₂			[Fe(**bppCONH₂**)₂](ClO₄)₂
Formula	$C_{24}H_{20}B_2F_8FeO_2N_{12}$	$C_{24}H_{20}B_2F_8FeO_2N_{12}$	$C_{24}H_{20}B_2F_8FeO_2N_{12}$	$C_{24}H_{20}Cl_2FeO_{10}N_{12}$
M_r	737.96	737.96	737.99	763.27
Crystal system	Monoclinic	Monoclinic	Monoclinic	Monoclinic
Space group	$P2_1/n$	$P2_1/n$	$P2_1/n$	$P2_1/n$
a/Å	9.24860(19)	9.25463(17)	9.3506(6)	9.4886(4)
b/Å	32.5567(8)	32.5863(6)	33.3034(10)	32.6089(8)
c/Å	10.3344(2)	10.5351(2)	10.8189(8)	10.5004(4)
α/°	90.000	90.000	90.000	90.000
β/°	109.892(8)	109.620(8)	107.8189(8)	109.721(4)
γ/°	90.000	90.000	90.000	90.000
V (Å³)	2926.06(18)	2992.66(17)	3212.85	3058.4(2)
Z value	4	4	4	4
μ (Mo-K$_\alpha$)/cm^{-1}	6.152	6.015	1.54184 (Cu-K$_\alpha$)	7.107
T/K	101	290	500	293
Measured reflections	27 559	29 045	18 409	15 661
Unique reflections	6634	6819	5715	7053
$R_1, I > 2\sigma(I)$	0.0489	0.0388	0.0575	0.0350
R, all data	0.0583	0.0507	0.0858	0.0745
wR, all data	0.1374	0.0967	0.1989	0.1648
Goodness of fit	1.056	1.033	1.008	1.033
CCDC deposit number	2085820	2085821	2085819	2085826
Spin state	LS	LS	HS/MS	LS

Fig. 1 Asymmetric unit of [Fe(**bppCONH₂**)₂](BF₄)₂ at 101 K with 50% thermal ellipsoids. Hydrogen atoms omitted for clarity.

longer than at 290 K (Table 2). In addition, the HS complex deviates more from ideal octahedral geometry with a ligand bite angle (α) of 75.05°, Σ value of 135.29° and Θ value of 456.84°, as in other HS state [Fe(**bpp**)₂]²⁺ complexes (see Table 2 for definitions). Although from DSC measurements (*vide infra*) at 500 K, the SCO event for the BF₄⁻ salt is not quite complete, therefore the 500 K structure may in fact represent a mixed spin-state (MS). Nevertheless, a comparison of the 290 and 500 K structures (Fig. 4) indicates that at 500 K the expected Jahn–Teller distortions, associated with HS state Fe(II) are in evidence. These changes are observed in a reduction of the α-angles and twisting out of plane with respect to the N$_{pyridyl}$–Fe–N$_{pyridyl}$ bond (Fig. 4 and Table 2).

Thermal analysis

Differential scanning calorimetry (DSC) can be used to estimate $T_{1/2}$ and quantify changes in enthalpy and entropy associ-

ated with the SCO phase change. The results of this analysis are given in Fig. 5. Both compounds exhibit a reversible broad transition. For [Fe(**bppCONH₂**)₂](ClO₄)₂ $T\uparrow$ (transition temperature on the heating cycle) is 459 K and $T\downarrow$ (cooling cycle) is 445 K giving a $T_{1/2}$ = 452 K. For the BF₄⁻ salt the values are $T\uparrow$ at 481 K and $T\downarrow$ at 461 K, $T_{1/2}$ being exceptionally high at 471 K. This data also shows that each compound shows hysteresis: 14 K for the ClO₄⁻ salt and 20 K for the BF₄⁻ salt. The DSC data for [Fe(**bppCONH₂**)₂](ClO₄)₂ reflects an incomplete transition due to restrictions imposed on the experimental temperature range, so ΔH and ΔS values were not calculated. By contrast at 525 K, the transition for the BF₄⁻ salt appears complete with ΔH ($T\uparrow$ 19.99, $T\downarrow$ 26.3 kJ mol⁻¹) and ΔS values ($T\uparrow$ 41.76, $T\downarrow$ 57.00 J K⁻¹ mol⁻¹). These transitions are less abrupt than for the corresponding thioamide derivatives.[9] The calculated values are consistent with SCO transitions in other [Fe(**bpp**)₂]²⁺ salts. However, it should be noted that DSC is not ideally suited to analyse broad SCO transitions since it is more difficult to determine a baseline to integrate the peaks and determine thermodynamic parameters.

SQUID magnetometry and Evans NMR

Typically, SCO is analysed in the solid-state by SQUID magnetometry to determine the variation in magnetic susceptibility as the sample is heated and cooled through the SCO transition. However, for the compounds reported here the high transition temperatures and maximum attainable experimental temperature in our magnetometer of 400 K mean that these measurements do not fully observe the HS state (Fig. 6 top). Nevertheless, both compounds show an increase in $\chi_m T$, starting at *ca.* 350 K, which can be attributed to the start of the SCO transition. At 400 K [Fe(**bppCONH₂**)₂](ClO₄)₂ shows a $\chi_m T$ value of 0.17 cm³ K⁻¹ mol⁻¹, corresponding to approximately 5% SCO completion (assuming $\chi_m T$ = 3.5 cm³ K⁻¹ mol⁻¹ at

Table 2 Selected bond lengths and bond angle parameters for Fe(II) coordination compounds of **bppCONH$_2$**, compared to values for HS and LS [Fe(**bpp**)$_2$](BF$_4$)$_2$

Structure	T (K)	Spin state	Bond lengths		Bond angle parameters				
			Fe–N$_{pyridyl}$ (Å)	Fe–N$_{pyrazolyl}$ (Å)	α^a (°)	Φ^b (°)	Σ^c (°)	Θ^d (°)	θ^e (°)
[Fe(**bpp**)$_2$](BF$_4$)$_2$ [21]	240	LS	1.893(3) 1.905(3)	1.979(3), 1975(3) 1.968(4), 1.981(3)	80.04	178.23 (1)	86.5	273.59	89.32
	290	HS	2.127(2) 2.125(2)	2.193(2), 2.184(3) 2.185(3), 2.175(3)	73.47	173.16 (8)	150.32	468.2	89.99
[Fe(**bppCONH$_2$**)$_2$] (ClO$_4$)$_2$	293	LS	1.891(3) 1.895(3)	1.969(4), 1.972(3) 1.965(4), 1.961(3)	80.25	177.1(1)	89.11	273.51	81.66
[Fe(**bppCONH$_2$**)$_2$] (BF$_4$)$_2$	101	LS	1.898(2) 1.894(2)	1.955(2), 1.961(2) 1.958(2), 1.962(2)	80.42	176.92 (2)	87.90	287.04	81.69
	290	LS	1.8955(14) 1.8922(14)	1.9608(17), 1.9622(17) 1.943(17), 1.9647(17)	80.30	177.4(1)	87.71	288.25	82.61
	500	HS/MS	2.068(3) 2.061(2)	2.092(3), 2.117(4) 2.109(5), 2.093(4)	75.05	174.1(1)	135.29	456.84	83.74

^{a} Average of four intra-ligand *cis*-N–Fe–N angles. ^{b} *trans*-N$_{pyridyl}$–Fe–N$_{pyridyl}$ angle. ^{c} Sum of the deviations from 90° of the 12 *cis*-N–Fe–N angles: larger value indicative of HS state. ^{d} Sum of the deviations from 60° of the 24 N–Fe–N angles, 6 angles per pseudo three-fold axis: larger values indicative of HS-state and deviation from O_h geometry towards D_{3h}.[22] ^{e} Angle between the mean planes of the 16 C and N atoms in each **bpp**-like ligand moiety: together with Φ an indication of Jahn–Teller distortion in the HS state. Typical values for these parameters for a range of **bpp** derivatives are given by Halcrow.[23] Σ and Θ were calculated using the OctaDist software version 2.6.[24]
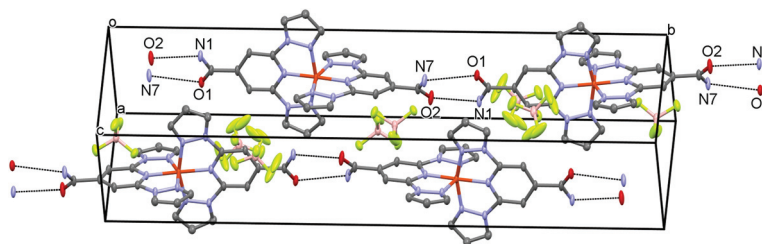
Fig. 2 Crystal packing of [Fe(**bppCONH$_2$**)$_2$](BF$_4$)$_2$ showing hydrogen bonded (dotted lines) forming 1D chains of cations.
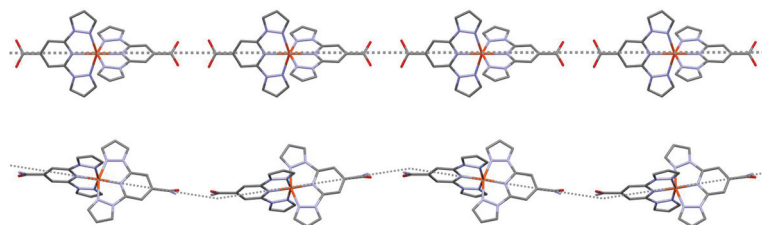
Fig. 3 The 1D chains in [Fe(**bppCOOH**)$_2$](BF$_4$)$_2$ (top) and [Fe(**bppCONH$_2$**)$_2$](BF$_4$)$_2$ (bottom). Both chains are viewed along the crystallographic *a*-axis. Dotted lines are a guide for the eye (crystallographic data of **bppCOOH** salt from García-López *et al.* ESI† [20]).
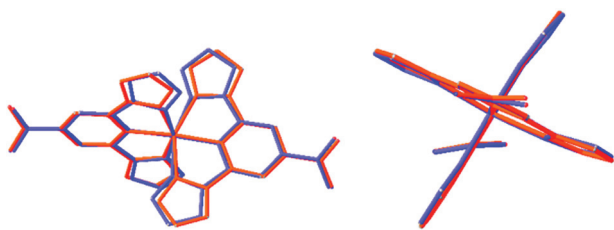
Fig. 4 Overlaid structure of the [Fe(**bppCONH$_2$**)$_2$] cation in the BF$_4^-$ salt at 290 K (LS, blue) and 500 K (HS, red).

100% HS state conversion). [Fe(**bppCONH$_2$**)$_2$](BF$_4$)$_2$ reaches a similar maximum but starts from a higher baseline paramagnetic contribution. Variable temperature magnetic susceptibility measurements using the Evans NMR method[25] confirm that both salts are SCO-active in CD$_3$NO$_2$ solution (Fig. 6 bottom). The compounds have a higher SCO transition temperature in solution than the prototypical [Fe(**bpp**)$_2$]$^{2+}$ salts but lower than [Fe(**bppCOOH**)$_2$]$^{2+}$.[26] This is consistent with a lower Hammett parameter for the amide group of 0.36 compared
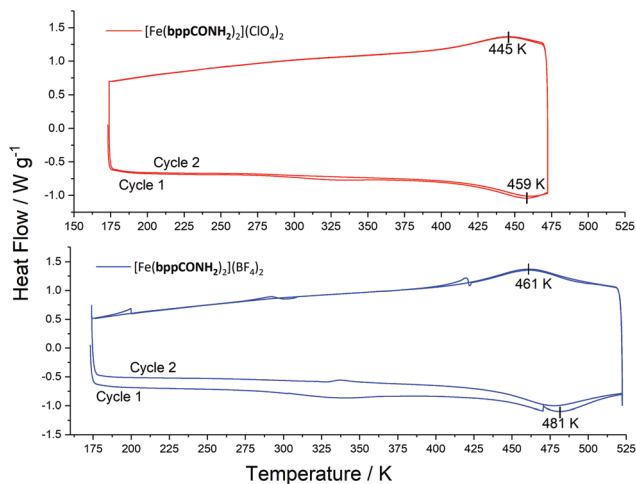
Fig. 5 DSC traces for [Fe(**bppCONH₂**)₂]²⁺ salts between 173 and 475 or 525 K, varying the temperature at a rate of 10 K min⁻¹.

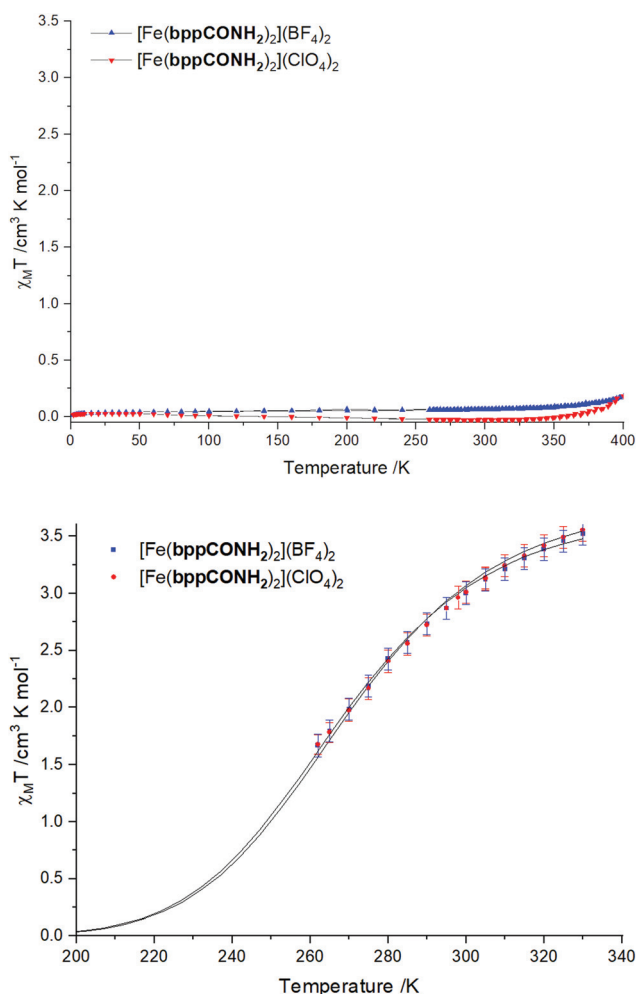**Fig. 6** Magnetic susceptibility multiplied by temperature *vs.* temperature ($\chi_m T$ *vs.* T) of the [Fe(**bppCONH₂**)₂]²⁺ salts determined in the solid-state by SQUID magnetometry (top) and in solution by Evans method[25] NMR in CD₃NO₂ (bottom). The solid line for the NMR data is a least-squares fit for SCO compounds as described by Rodriguez-Jimenez.[28]

with that for carboxylic acid in the same position with 0.45.[27] The expected result is a reduced electron withdrawing effect and increased basicity of the pyridyl-N lone pair but reduced π-acceptor character of the **bppCONH₂** ligand.

Variable temperature Raman spectroscopy

Additional evidence for the SCO transition in [Fe(**bppCONH₂**)₂] (BF₄)₂ was attempted using variable temperature powder X-ray diffraction under a nitrogen atmosphere. However, during measurement over extended periods at high temperatures this material eventually carbonises (Fig. S2†). Therefore, variable temperature Raman spectroscopy under a nitrogen atmosphere was attempted. This technique also allows simultaneous visualisation of the thermochromism that accompanies an SCO-event. The results are shown in Fig. 7. Equivalent analysis of [Fe(**bppCONH₂**)₂](ClO₄)₂ was not attempted due to the potential of explosion in the spectrometer's sample chamber.

[Fe(**bppCONH₂**)₂](BF₄)₂ was initially heated to 323 K (50 °C) where a photograph of the LS state single crystal was obtained, which had a distinct red/brown colour (Fig. 7). The sample was then heated to 518 K (245 °C) in steps of 5–10 K. As the temperature increased there was an increase in intensity of the band at 1015 cm⁻¹ and a simultaneous reduction of the band at 1037 cm⁻¹, assigned to the HS and LS states, respectively. This assignment corresponds to other studies looking at Raman spectra and SCO in **bpp**-derivatives.[15,29] The intensity of the 1015 cm⁻¹ band at each temperature was divided by its intensity at 518 K, with the assumption that the HS fraction was 100% at 518 K. This assumption is based on DSC data which shows that the SCO event is completed above 510 K. To compensate for small defocussing of the laser as the temperature changes, the intensities were corrected by normalising to the intensity of unchanged peaks. The data, plotted as HS state fraction (γHS) *vs.* temperature (Fig. 7 bottom) is consistent with the DSC data, showing the start of an SCO event at 400 K with an estimate of $T_{1/2}$ of 475 K. On face value the Raman also indicates a hysteresis between heating and cooling traces, supporting the DSC data. However, this must be treated with caution since the experiment required re-centring and re-focussing during the data collection, together with the possibility of local heating from the laser. Nevertheless, it is clear that the Raman data shows that am SCO event occurs at the expected temperature. The SCO is supported by the observation of a reversibly change in colour between red/brown (LS) and light orange (HS), which is expected for an SCO transition of a Fe(II) complex with **bpp**-like ligands. In addition, the presence of hysteresis in a compound with a gradual SCO transition is quite unusual, although not unknown, since abrupt transitions and hysteresis are both consequences of intermolecular cooperativity. If hysteresis is present, as shown in the DSC, it is speculated that the effect might be attributed to the non-symmetrical hydrogen bonding of the amide groups within the 1D chains. As noted above, this promotes wave-like 1D chains and asymmetrical changes to the lengths of the hydrogen bonds as the temperature is varied. At 500 K, the
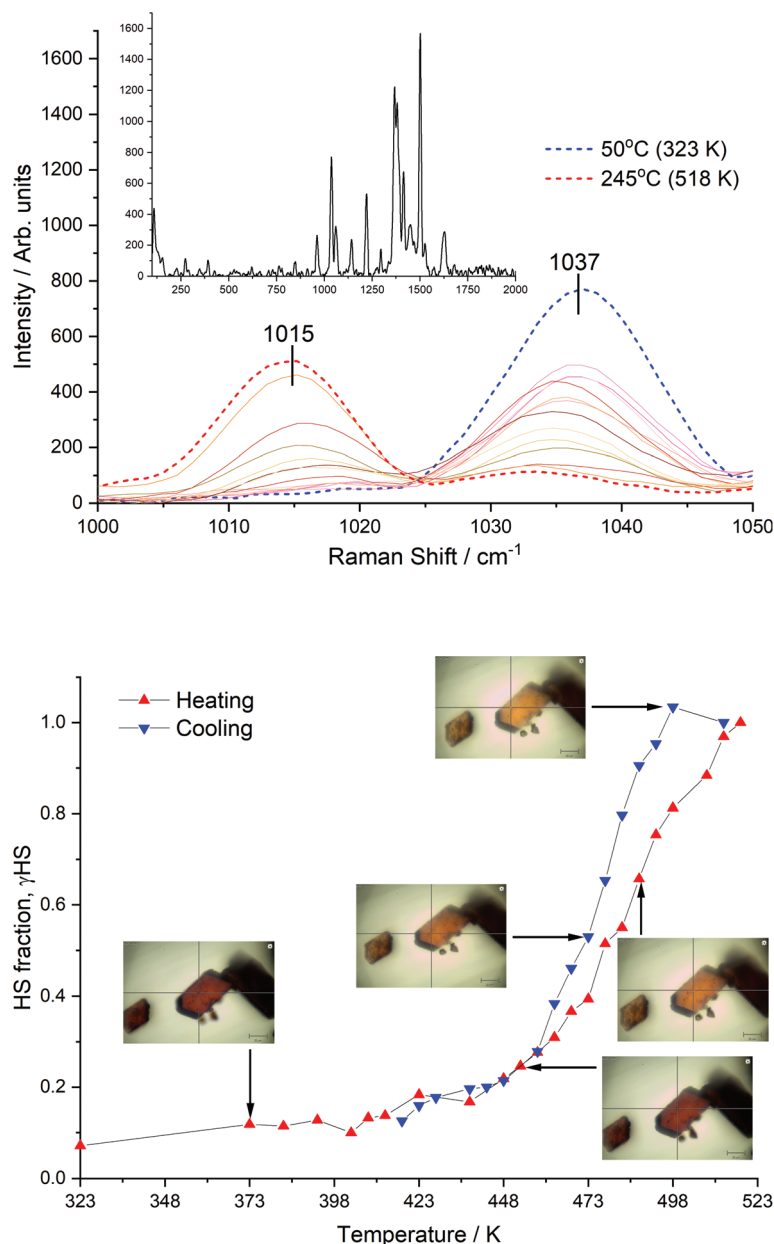
Fig. 7 Variable temperature Raman spectra of [Fe(**bppCONH₂**)₂](BF₄)₂ at 633 nm excitation showing the 1000 to 1050 cm⁻¹ region (top), highlighting spectra of the LS (323 K) and HS (518 K) species (dotted lines). Inset shows full range spectrum at 323 K. Plot of HS fraction *vs.* temperature with associated photographs of the crystals (bottom, see text for details).

shortest hydrogen bond measures 3.14 Å, which is relatively weak. Therefore, stronger cation–cation interactions are present at the start of the heating cycle, but these interactions are weaker at the start of the cooling cycle. Consequently, on the cooling cycle the HS state could be more stabilised following the SCO transition. These Raman data in combination with single crystal X-ray diffraction and DSC identifies the presence of very high temperature SCO transitions in the **bppCONH₂** based materials. Furthermore, DSC indicates the presence of hysteresis, which should be confirmed, for example with high temperature SQUID measurements.

Conclusion

It has been observed that Fe(ɪɪ) coordination entities with **bpp**-like ligands and cationic 1D chain structures can exhibit high temperature SCO transitions. In complexes of the ligand **bppCOOH** linear 1D chains form due to inter-cationic hydrogen bonding, which has been considered to stabilise the LS state and thereby increase the SCO transition temperature to 380 K. This is typically above the SCO transition temperature of **bpp**-containing compounds that rely on inter-cationic π–π stacking. We have previously been able to moderate the SCO

temperature towards room temperature with thioamide-based ligands **bppCSNHMe** and **bppCSNH$_2$**. In the present work using amide-based **bppCONH$_2$** provided further insight into how peripheral functionalisation of the ligand can affect the transition behaviour. In this case it has been observed that reducing the structural rigidity of the hydrogen-bonded network leads to a gradual SCO transition. However, high transition temperatures and possible hysteresis are also observed. It is speculated that hysteresis could be present due to a difference in strength of hydrogen bonding in the HS and LS states. Variable temperature Raman spectroscopy has proven useful to characterise the SCO events, particularly at such high temperatures. Future investigations will focus on moderating the hydrogen bonding networks to investigate the effect on the nature and temperature of the SCO transition.

Author contributions

MA synthesised the compounds and performed or assisted in all characterisation experiments, with the exception of the single crystal XRD and elemental analyses. MA also wrote the first draft of the manuscript. HA collected and analysed the SQUID data, and collected XRD data and solved structures of the BF$_4$ salts at 101 and 290 K. LM and TB collected XRD data and solved the structure of the ClO$_4$ salt. PLM collected the XRD data and solved the structure of the BF$_4$ salt at 500 K. SST initiated the research, obtained funding, supervised the work and edited all versions of the manuscript after the initial draft.

Conflicts of interest

There are no conflicts of interest.

Acknowledgements

Notes and references

1 M. A. Halcrow, *Polyhedron*, 2007, **26**, 3523–3576.

2 L. J. K. Cook, H. J. Shepherd, T. P. Comyn, C. Baldé, O. Cespedes, G. Chastanet and M. A. Halcrow, *Chem. – Eur. J.*, 2015, **21**, 4805–4816.

3 M. A. Halcrow, I. C. Berdiell, C. M. Pask and R. Kulmaczewski, *Inorg. Chem.*, 2019, **58**, 9811–9821.

4 A. Abhervé, M. Clemente-León, E. Coronado, C. J. Gómez-García and M. López-Jordà, *Dalton Trans.*, 2014, **43**, 9406–9409.

5 (*a*) M. L. Scudder, H. A. Goodwin and I. G. Dance, *New J. Chem.*, 1999, **23**, 685–705; (*b*) R. Pritchard, C. A. Kilner and M. A. Halcrow, *Chem. Commun.*, 2007, 577–579.

6 I. Šalitroš, O. Fuhr, A. Eichhofer, R. Kruk, J. Pavlik, L. Dlháň, R. Boča and M. Ruben, *Dalton Trans.*, 2012, **41**, 5163–5171.

7 M. Halcrow, I. C. Berdiell, C. M. Pask and R. Kulmaczewski, *Inorg. Chem.*, 2019, **58**, 9811–9821.

8 I. Šalitroš, J. Pavlik, R. Boča, O. Fuhr, C. Rajadurai and M. Ruben, *CrystEngComm*, 2010, **12**, 2361–2368.

9 M. Attwood, H. Akutsu, L. Martin, D. Cruickshank and S. S. Turner, *Dalton Trans.*, 2019, **48**, 90–98.

10 N. Bridonneau, L. Rigamonti, G. Poneti, D. Pinkowicz, A. Forni and A. Cornia, *Dalton Trans.*, 2017, **46**, 4075–4085.

11 A. Abhervé, M. Palacios-Corella, J. M. Clemente-Juan, R. Marx, P. Neugebauer, J. van Slageren, M. Clemente-León and E. Coronado, *J. Mater. Chem. C*, 2015, **3**, 7936–7945.

12 E. Brunet, O. Juanes, R. Sedano and J.-C. Rodríguez-Ubis, *Photochem. Photobiol. Sci.*, 2002, **1**, 613–618.

13 A. K. Botcha, S. Basak and R. Chandrasekar, *RSC Adv.*, 2014, **4**, 34760.

14 M. Cavallini, I. Bergenti, S. Milita, J. C. Kengne, D. Gentili, G. Ruani, I. Salitros, V. Meded and M. Ruben, *Langmuir*, 2011, **27**, 4076–4081.

15 H. Shepherd, G. Tonge, L. Hatcher, M. Bryant, J. Knichal, P. Raithby, M. Halcrow, R. Kulmaczewski, K. Gagnon and S. Teat, *Magnetochemistry*, 2016, **2**, 9.

16 H. Shepherd, P. Rosa, L. Vendier, N. Casati, J. F. Létard, A. Bousseksou, P. Guionneau and G. Molár, *Phys. Chem. Chem. Phys.*, 2012, **14**, 5265–5271.

17 G. A. Bain and J. F. Barry, *J. Chem. Educ.*, 2008, **85**, 532–536.

18 M. Adamczyk, S. R. Akireddy and R. E. Reddy, *Tetrahedron*, 2002, **58**, 6951–6963.

19 T. Vermonden, D. Branowska, A. T. M. Marcelis and E. J. Sudhölter, *Tetrahedron*, 2003, **59**, 5039–5045.

20 V. García-López, M. Palacios-Corella, A. Abhervé, I. Pellicer-Carreño, C. Desplanches, M. Clemente-León and E. Coronado, *Dalton Trans.*, 2018, **47**, 16958–16968.

21 J. M. Holland, C. A. Kilner, M. Thornton-Pett, M. A. Halcrow, J. A. McAllister and Z. Lu, *Chem. Commun.*, 2001, 577–578.

22 (*a*) J. K. McCusker, A. L. Rheingold and D. N. Hendrickson, *Inorg. Chem.*, 1996, **35**, 2100–2112; (*b*) P. Guionneau, M. Marchivie, G. Bravic, J.-F. Létard and D. Chasseau, *Top. Curr. Chem.*, 2004, **234**, 97–128.

23 M. A. Halcrow, *Coord. Chem. Rev.*, 2009, **253**, 2493–2514.

24 R. Kerkaew, Y. Tantirungrotechai, P. Harding, G. Chastanet, P. Guionneau, M. Marchivie and D. J. Harding, *Dalton Trans.*, 2021, **50**, 1086–1096. Software available at https://octadist.github.io.

25 D. F. Evans, *J. Chem. Soc.*, 1959, 2003–2005.

26 L. J. K. Cook, R. Kulmaczewski, R. Mohammed, S. Dudley, S. A. Barrett, M. A. Little, R. J. Deeth and M. A. Halcrow, *Angew. Chem., Int. Ed.*, 2016, **55**, 4327–4331.

27 C. Hansch, A. Leo and R. W. Taft, *Chem. Rev.*, 1991, **91**, 165–195.

28 S. Rodriguez-Jimenez and S. Brooker, *Inorg. Chem.*, 2017, **56**, 13697–13708.

29 A. Abhervé, M. J. Recio-Carretero, M. López-Jordà, J. M. Clemente-Juan, J. Canet-Ferrer, A. Cantarero, M. Clemente-León and E. Coronado, *Inorg. Chem.*, 2016, **55**, 9361–9367.